Fibers and Polymers 2019, Vol.20, No.4, 698-708
DOI 10.1007/s12221-019-1092-1

ISSN 1229-9197 (print version)
ISSN 1875-0052 (electronic version)

Characteristics, Controlled-release and Antimicrobial Properties of Tea Tree Oil Liposomes-incorporated Chitosan-based Electrospun Nanofiber Mats

Yan Ge[1,2], Jiapeng Tang[3]*, Haihong Fu[1,2], Yijun Fu[1,2], and Yuanyuan Wu[4]

[1]*School of Textile and Clothing, Nantong University, Nantong 226019, PR China*
[2]*National & Local Joint Engineering Research Center of Technical Fiber Composites for Safety and Protection, Nantong University, Nantong 226019, PR China*
[3]*Institute of Special Environmental Medicine, Nantong University, Nantong 226019, PR China*
[4]*Xinglin College, Nantong University, Nantong 226007, PR China*

(Received November 14, 2018; Revised December 31, 2018; Accepted January 3, 2019)

Abstract: In this paper, a notable chitosan/poly(ethylene oxide) nanofiber mats containing tea tree oil liposomes (TOL-CENs) were successfully fabricated using electrospinning process. The microstructures and morphology were characterized by scanning electron microscopy. The porosity, fluid absorbability, water vapor permeability and mechanical properties of nanofiber mats were also estimated by ethanol density method, gravimetric method, dish method and tensile test, respectively. Compared to the chitosan/poly(ethylene oxide) composite freeze-dried sponges containing tea tree oil liposomes, TOL-CENs had greater porosity, water absorption, breathability and better mechanical properties. In addition, the controlled-release properties and long-term bactericidal capability of the material were also assessed. From the analysis of the release kinetics and mechanism, it was found that the significant decreased terpinen-4-ol concentration gradient from liposomal surface to the outside of material was the key to the sustained terpinen-4-ol release in virtue of liposomal encapsulation. TOL-CENs exhibited long-term and more excellent microbicidal effects against *Staphylococcus aureus*, *Escherichia coli* and *Candida albicans* than chitosan/poly(ethylene oxide) nanofiber mats. The combination of tea tree oil liposomes and chitosan in nanofiber mats synergistically destroyed cell membrane, prevented cell adhesion and caused the irregular aggregation of cytoplasm, resulting in cell disintegration observed by transmission electron microscope. In summary, TOL-CENs had potential application value as a long-term antimicrobial nonwoven materials.

Keywords: Chitosan/PEO nanofiber, Tea tree oil liposomes, Electrospinning, Controlled release, Long-term antimicrobial property

Introduction

Various fabrics are susceptible to contact organic stains and dust, and become a good environment for the growth and reproduction of microbes, especially bacteria and molds. The fabrics used in hospitals and hotels provide conditions for disease transmission and cross-contamination caused by pathogens. The hygienic problems of nonwoven materials applied in apparel, health care and decoration attract considerable attention. In order to resolve this problem, the antimicrobial agents-loading nanofibers as an important antimicrobial nonwoven materials (ANMs), have been developed for filtration, paint, food packaging, drug delivery vehicles, tissue engineering, biofilms and sensors [1-9]. At present, antimicrobial agents mainly include organic antimicrobial agents (antibiotics, quaternary ammonium and biguanide biocides) [10-12] and inorganic antimicrobial agents (nanosilver and metal oxides) [13,14].

Tea tree oil is a kind of volatile natural plant essential oil. It is obtained by steam distillation of the leaves and terminal branches of the Australian native plant *Melaleuca alternifolia*, which is usually used to treat skin infections [15]. Terpinen-4-ol is one of the main physiological active components of tea tree oil and has significant activity in inhibiting and killing microorganisms. Its content levels are 30 % to 48 % in tea tree oil [15]. However, tea tree oil is highly volatile and oxidized by light, temperature and air [16]. It has been reported that human skin is sensitized to the oxidized tea tree oil [17,18]. Therefore, it is an alternative strategy to load tea tree oil into the drug controlled-release system to protect and release it [19].

Due to the biodegradability, biocompatibility, antibacterial activity, low immunogenicity and good wound healing ability, chitosan nanofibers have attracted widespread attention and showed good physical and biological properties [20, 21]. Pure chitosan electrospun fibers can only be performed in concentrated acetic acid or trifluoroacetic acid, which limits its application in drug controlled-release systems [22-24]. Currently, the biodegradable and biocompatible blend electrospun fibers such as chitosan/poly(ethylene oxide) (PEO) nanofibers [25,26] and chitosan/polyvinyl alcohol (PVA) nanofibers [27,28] are prepared so that to achieve the balance of spinnability, functionality and biological properties. In addition, chitosan electrospun fiber mats have high porosity and specific surface area. Because of the good hydrophilicity, chitosan electrospun fiber mats as the controlled-release system of hydrophobic drugs, will cause the significant burst effects and shorten the antimicrobial duration of materials.

*Corresponding author: jptang@ntu.edu.cn

However, the ideal antimicrobial nanofibers should have both efficient antimicrobial effects and long-term antimicrobial duration, so we developed tea tree oil liposomes. Liposomes are self-assemblies of lipid molecules and the structure in which one or more lipid bilayers coat the mini-water phase. As a drug controlled-release system, liposomes can either carry hydrophilic drugs in the micro-aqueous phase, or carry lipophilic drugs in the bilayer membrane [29,30]. As a drug carrier, liposomes achieve the sustained release of drugs, decrease the dose of drug delivery and improve the bioavailability of drugs, simultaneously also reduce the toxic side effects of drugs on non-pathogenic tissues by modulating pharmacokinetics and biodistribution of drugs [31]. Essential oil liposomes can protect essential oil and enhance the solubility of essential oil in water [16], so they have many applications *in vivo* and *in vitro* [16]. In addition, liposomes can improve antimicrobial activity of encapsulated essential oil [16]. For example, carvacrol and thymol are the main components of oregano oil, and their antimicrobial activity was significantly enhanced after being encapsulated in liposomes, which promoted carvacrol and thymol liposomes as highly effective preservatives and protective agents used in the fields of foods, cosmetics and pharmaceutical industry [32]. When *Artemisia arborescens* essential oil was wrapped in multilayer large vesicles, its antiherpetic activity was improved. These multilayer large vesicles enhanced the targeting of essential oil to pathogens [33]. *Eucalyptus camaldulensis* essential oil was encapsulated in liposomes to increase the antifungal activity significantly [34]. The incorporation of *Artemisia annua* oil liposomes and clove oil/chitosan nanoparticles into the edible agar films containing chitosan and gelatin nanofibers possessed bacteriostatic effect against *E. coli* O157:H7 [35,36], respectively. The incorporation of cinnamon essential oil/β-cyclodextrin proteoliposomes into PEO nanofibers can inhibit the growth of *Bacillus cereus* on beef [37]. The gelatin nanofibers containing thyme essential oil/β-cyclodextrin epsilon-polylysine nanoparticles showed excellent antimicrobial activity against *Campylobacter jejuni*, which caused membranolysis and protein leakage of *C. jejuni* [38]. The tea tree oil liposomes/chitosan nanofibers can prevent the microbial contamination by *Salmonella* spp. [39]. In the previous study, we incorporated tea tree oil liposomes and eucalyptus essential oil liposomes into chitosan to prepare tea tree oil liposomes/chitosan composite sponges and eucalyptus essential oil liposomes/chitosan composite sponges by freeze-dried method [40,41]. The addition of tea tree oil liposomes and eucalyptus essential oil liposomes increased the antimicrobial effects against *Staphylococcus aureus* (*S. aureus*), *Escherichia coli* (*E. coli*) and *Candida albicans* (*C. albicans*), and antimicrobial property of the materials was enhanced with the increasing of essential oil liposomes concentration.

In this study, tea tree oil liposomes-incorporated chitosan-based electrospun nanofiber mats (TOL-CENs) were developed to strengthen the interaction between chitosan and drugs and weaken the burst effect. The performances, drug release kinetics and antimicrobial effects of TOL-CENs were compared with the tea tree oil liposomes-incorporated chitosan-based freeze-dried sponges (TOL-CFSs). The release behavior of terpinen-4-ol in TOL-CENs was analyzed by comparison of drug release kinetics so that to reveal the drug sustained-release mechanism and antimicrobial mechanism.

Experimental

Materials

Chitosan (CS, average Mw 500,000 Da, 85 % deacetylation degree), PEO (average Mw 8,000 Da), Soybean phosphatidylcholine (PC), cholesterol (Chol) and Tween-80 were obtained from Sinopharm Chemical Reagent Co., Ltd. (Shanghai, China). Tea tree oil (TTO) was purchased from Nanning Innovative Pharmceutical Technology Co., Ltd. (Nanning, China). Concentrations of the TTO components determined by gas chromatographic analysis (and the range specified by the international standard ISO 4730:1996, shown in parentheses) were as follows: 2.75 % α-pinene (1-6 %); 0.53 % sabinene (trace to 3.5 %); 9.79 % α-terpinene (5-13 %); 1.05 % limonene (0.5-4 %); 2.19 % p-cymene (0.5-12 %); 2.9 % 1,8-cineole (0-15 %); 18.91 % γ-terpinene (10-28 %); 3.11 % terpinolene (1.5-5 %); 46.96 % terpinen-4-ol (>30 %); 2.56 % α-terpineol (1.5-8 %); 0.6 % aromadendrene (trace to 7 %); 0.44 % δ-cadinene (trace to 8 %); 0.26 % globulol (trace to 3.5 %); and 0.29 % viridiflorol (trace to 1.5 %). All the other chemicals used were also of analytical grade. The water used for experiments was obtained by double distillation of deionized water.

Preparation of Tea Tree Oil Liposomes (TTOLs)

TTOLs was fabricated from PC, Chol and TTO using the conventional thin film hydration method as described by Ge *et al.* [19]. Briefly, 100 mg PC and 20 mg Chol were dissolved in 10 m*l* chloroform in a dry round bottom flask and the solvent was evaporated at room temperature, 12 rpm for 1 h using a rotary evaporator. The remaining lipid-film was hydrated with 10 m*l* TTO solution (phosphate-buffered saline (PBS), pH 3.0, containing 1.0 vt% (volume percentage) Tween-80 and 2.0 vt% TTO) by agitation for 20 min at 45 ^{o}C. Simultaneously, the sonication was carried out in a bath-type sonicator (Branson Ultrasonics, Danbury, CT, USA) to form small unilamellar liposomes. Finally the liposomal dispersions prepared were stored at room temperature for 3 h in order to anneal any structural defects. According to the methods mentioned in the literature [19], the encapsulation efficiency of TTOLs prepared was 98.49± 1.29 % and terpinen-4-ol concentration in TTOLs suspension was 0.92±0.03 wt% for the preparation of materials.

Fabrication of TOL-CENs and TTO-CENs

Chitosan and PEO powders were mixed at a weight ratio of 90:10 and then dissolved in 90 vt% aqueous acetic acid at a polymer concentration of 4.0 wt%. The mixtures were stirred at room temperature for 12-24 h with a magnetic stirrer to ensure complete dissolution of the polymers and obtain homogeneous solutions. The prepared solutions were left to rest for 1 h for degassing and kept in sealed containers at room temperature. TTOLs suspension was added to the polymer solutions at a concentration of 2.0 vt% to obtain the electrospinning solution. The electrospinning solution was transferred to a 10-m*l* syringe pump with a stainless steel needle (blunt tip, gauge 21) attached to it. The resulting fibers were collected on a grounded aluminum plate to obtain TOL-CENs. All of the electrospinning processes were carried out at 15 °C and 50-70 % RH. The solution flow rate was 0.5 m*l*/h, a positive voltage range of 15 kV was applied to the collecting target by a high-voltage power supply, and the distance between needle tip and the target was 20 cm.

For comparison, TTO solution was added to the polymer solutions at a concentration of 2.0 vt% instead of TTOLs suspension and TTO-CENs were prepared by the same electrospinning method. PBS solution was added instead of TTOLs suspension and chitosan-based electrospun nanofiber mats (CENs) were also fabricated as a control.

Fabrication of TOL-CFSs and TTO-CFSs

TOL-CFSs and TTO-CFSs were prepared according to the method in the literature [40]. Briefly, chitosan and PEO powders were mixed at a weight ratio of 90:10 and then dissolved in 2.0 vt% acetic acid solution at a polymer concentration of 4.0 wt% to obtain homogeneous CS/PEO solution. Then, TTOLs suspension was mixed with CS/PEO solution at a concentration of 2.0 vt% to obtain the resulting casting solution. The casting solution was poured into a clean, sterile, glass Petri dish and placed in a vacuum freeze-drying machine, pre-freezed in -5 °C for 3 h, then cooled to -55 °C at the speed of 5 °C/h and maintained 30 min, and cooled to -80 °C, freeze-dried for 72 h. The degree of vacuum maintained at less than 0.012 mBar. Finally, TOL-CFSs were successfully fabricated. TTO-CFSs were also prepared using the TTO solution instead of TTOLs suspension by the same freeze-dried method. PBS solution was added into CS/PEO solution instead of TTOLs suspension and chitosan-based freeze-dried sponges (CFSs) were also prepared as a control.

Transmission Electron Microscopy (TEM)

The morphology of TTOLs before and after mixing with the polymer solution were studied using a transmission electron microscope (TEM; JEM-2100, Tokyo, Japan). Briefly, the liposomes before and after mixing with the polymer solution diluted ten-fold in water was deposited on a sample grid (carbon membrane supported by a copper grid) and negatively stained with phosphotungstic acid solution 2.0 % (w/v). All preparations were allowed to dry for 2 h and then observed with JEM 2100 TEM operating at an accelerating voltage of 100 kV.

Scanning Electron Microscopy (SEM)

The morphology of samples was observed by SEM (JSM-6510, JEOL, Japan). Samples were sliced into thin sections and then gold sputtered before SEM imaging. Diameter range and morphology of nanofibers has been analyzed from ten different positions.

Fourier Transform Infrared Spectroscopy (FTIR)

The FTIR spectra of samples were recorded using a FTIR Spectrometer (Nicolet iS50, Thermo Scientific, US) at the range of 400-4000 cm^{-1}.

Differential Scanning Calorimetry (DSC)

The dynamic thermal behaviors of samples were analyzed using a simultaneous thermal analyzer (DSC/DTA-TG, STA 449 F5, NETZSCH, Germany) under a N_2 atmosphere with a heating rate of 10 °C/min from 25 °C to 380 °C.

X-ray Diffraction (XRD)

The XRD patterns of samples were obtained at room temperature using a multipupose X-ray diffractometer (Ultima IV, Rigaka, Japan) with CuKα radiation at a voltage of 40 kV. XRD were taken at 2θ range of 10-80 °C and scanned at a speed of 5 ° min^{-1}.

Zeta Potential of the Mixture of TTOLs and Polymer Solution

TTOLs suspension was mixed with polymer solution in a certain ratio and then the mixture was diluted with water to the appropriate concentration. Zeta potential of the obtained mixture was measured by Zetasizer (Nano ZS90, Malvern, UK).

Measurements of Porosity, Fluid Absorption and Water Vapor Transmission Rate

The porosity of materials was determined on the basis of the Archimedes principle [40]. The sample was weighed and immersed in ethanol at 37 °C for 24 h. The resulting sample was withdrawn and the wet weight of sample was measured after removing excess surface ethanol of sample with a filter paper. Then, the wet sample was added into the pycnometer filling with ethanol and weighed. Porosity was calculated using equation (1):

$$Porosity\ (\%) = \frac{w_1}{w_2} \times 100 \quad (1)$$

where w_1 is the weight of ethanol in the sample, g; w_2 is the weight of the ethanol discharged by the wet sample in the

pycnometer, g.

The samples were weighed and totally immersed in PBS solution (pH 7.4) at 37 °C for 24 h. The resulting sample was withdrawn and weighed after removing its excess surface liquid with filter paper. Fluid absorption (FA) of samples was calculated according to the following formula:

$$FA = \frac{w_3}{w_4} \quad (2)$$

where *FA* is fluid absorption, $g \cdot g^{-1}$; w_3 is the weight of PBS solution in the sample, g; w_4 is the wet weight of the sample, g.

The water vapor transmission rate (WVTR) of matrerials was measured as described by Ge *et al.* [40]. Briefly, A sufficient amount of water was added to the high-type weighing bottle (25 mm in diameter) so that the distance from liquid surface to the top of bottle was 5±1 mm. The circular sample was fastened over the top of weighing bottle and accuratly weighed. The weighing bottle was kept at 37±1 °C and 10 % RH. After a period of time, the weighing bottle was taken out and re-weighed. WVTR was calculated by the following equation:

$$WVTR = \frac{w_5}{S \cdot T} \quad (3)$$

where *WVTR* is water vapor transmission rate, $g \cdot m^{-2} \cdot d^{-1}$; w_5 is the weight of reduced water in the cup, g; *S* is the area of the rim of cup, m^2; *T* is the experimental time, d.

Mechanical Property

The Young's modulus and elongation at break of the sample in the wet state was measured using intelligent electronic tensile machine (XLW (G)-PC, Labthink, CN). The sample was immersed in PBS solution for 24 h and cut into 50 mm in length. The stretching rate was 10 mm/min.

***In vitro* Terpinen-4-ol Release in Polymer Carrier**

Terpinen-4-ol is an important active component of TTO. The chemical compositions of TTO were determined by GC-MS (Agilent 7890B-7000C, USA) [29]. The GC system was equipped with a Agilent Technology HP-5ms (5 % phenyl methyl siloxane) column (30 m×0.25 mm i.d.; film thickness 0.25 μm) for separation. The volume of the injected sample was 0.2 μ*l*. Hydrogen (1 m*l*/min) was used as a carrier gas and the split ratio was 1:10. The injector temperature and detector temperature were 280 °C. The oven temperature programme was 60 °C for 2 min, then 10 °C/min until 280 °C was reached, and maintained 2 min. Using n-dodecane as internal standard, the calibration factors of TTO components were measured.

To measure TTO release from the materials, a known area (2 cm×2 cm) of samples weighed was placed in Erlenmeyer flask and added 100 m*l* PBS solution, then shaked at 150 rpm in 37 °C. Terpinen-4-ol release of samples was observed over 7 days. 0.2 m*l* buffer was removed for 2, 4, 8, 12, 24, 48, 72, 120, 168 h and substituted with fresh buffer to measure the concentration of released TTO using gas chromatography. The release experiments of each sample were performed in triplicate and average values were reported. The accumulative release rate of TTO from the materials was calculated using the following equation (4):

$$CTR\ (\%) = \left(\frac{C_T V_p}{W_T m}\right) \times 100 \quad (4)$$

where *CTR* is the accumulative release rate of TTO, %; C_T is terpinen-4-ol concentration in PBS, g/m*l*; V_p is PBS volume, m*l*; W_T is terpinen-4-ol quality concentration in the samples, g/g; *m* is the sample quality, g.

Study of Terpinen-4-ol Release Kinetics and Mechanism

The release kinetics of terpinen-4-ol from a polymer carrier can be described using five most common kinetic models which are zero order, first order, Hixson-Crowell model, Higuchi model and Korsmeyer-Peppas model (equations (5)-(9)). In addition, Kim *et al.* modified the Korsmeyer-Peppas model by introducing the concept of delay time [42-44]. On this basis, the further modified Korsmeyer-Peppas model after estimating the burst effect (see below). All of these models explained the release pattern to be dependent on some individual property.

Zero order model: $$M_t = k(t - t_{lag}) + M_0 \quad (5)$$

First order model: $$\ln(1 - M_t) = k(t - t_{lag}) + M_0 \quad (6)$$

Hixson-Crowell model: $$M_t = k(t - t_{lag})^3 + M_0 \quad (7)$$

Higuchi model: $$M_t = k(t - t_{lag})^{0.5} + M_0 \quad (8)$$

The modified Korsmeyer-Peppas model:

$$M_t = k(t - t_{lag})^n + M_0 \quad (9)$$

where M_t is the terpinen-4-ol released ratio at time t; M_0 is the initial terpinen-4-ol released ratio at 0 h; t_{lag} is the lag time of terpinen-4-ol release; *k* represents the release rate constant of the model; *n* is the release exponent of model fitting.

Microbiocidal Properties

Microbiocidal activity was assessed according to the killing log value (KLV) of TOL-CENs and CENs against Gram positive bacteria (*S. aureus* ATCC 6538), Gram-negative bacteria (*E. coli* ATCC 8739) and fungi (*C. albicans* ATCC 10231). The sample (a wafer of 1 cm diameter) was put in 50 m*l* of liquid culture diluted to 5×10^7 cfu/m*l* with Luria-Bertani (LB) broth (*S. aureus* and *E. coil*) and yeast malt (YM) medium (*C. albicans*). Then the culture was incubated at 37 °C on a rotary shaker at 250 rpm for 1, 3,

6 days. Afterwards, the living cell concentration was observed by a dilution plate counting method. KLV of TOL-CENs was calculated as followed:

$$KLV = \log_{10}N_0 - \log_{10}N_t \quad (10)$$

where KLV is the killing log value; N_0 is the number of microorganism in broth at 0 contact time, cfu/m*l*; N_t is the number of microorganism in broth at the time, cfu/m*l*.

TEM Observation of Microbial Cell Structure

S. aureus, *E. coli* and *C. albicans* cell suspensions were treated with TOL-CENs and CENs for 24 h and then cells were collected by centrifugation. After appropriate dilution of microbial cells, the sample was deposited on a carbon-coated copper grid and negatively stained with 2.0 wt% phosphotungstic acid solution. The ultrastructure of microbial cells was then observed by transmission electron microscope (TEM, JEM-2100, Tokyo, Japan) operating at an accelerating voltage of 100 kV. The untreated microbial cell suspensions were observed as a control.

Data and Statistical Analyses

The experimental results were expressed as the mean of mutiple trials ±SD (standard deviation). Differences were considered statistically significant when $p<0.05$ (two-sided). Statistical analysis of the generated data was performed using GraphPad Prism 5.0 (San Diego, CA).

Results and Discussion

Morphology and Structure of TOL-CENs and TOL-CFSs

Figure 1 displays the morphology of liposomes before and after mixing with the polymer solution. The particle size of TTOLs prepared in PBS (pH 3.0) was 50-100 nm, which was similar to the particle size of liposomes prepared in PBS (pH 7.4) [19]. When TTOLs were added to the polymer solution, the polymer was coated on the surface of liposomes and the particle size greatly increased to 150-300 nm. The thicker polymer shell may contribute to the stabilization of TTO.

Figure 2 shows the SEM images of CENs and CFSs with and without TTOLs. Seen in Figure 2(A), CFSs were the multilayered porous sponge-like materials. During the formation of CFSs, the polymer matrix absorbed water, swelled and was converted into the hydrogel. The phase separation between water and polymer occurred in the freezing condition, then the freezed ice was sublimed away under vacuum to leave holes. These holes communicated with each other and extended into the interior of materials [45,46]. After adding TTOLs, the liposomes inserted among chitosan molecules, so the micro-surface structure of CFSs became much rougher but the pore structure remained intact [40]. The average pore size of material surface is 152±54 μm (Figure 2(B)).

CENs were also successfully electrospun by 4.0 wt% polymer solution with CS/PEO mass ratios of 90:10. As displayed in Figure 2(C), the prepared CENs were composed of continuous, fine, cylindrical fibers without bead structure, consistent with the morphology previously reported [26,47] and had average fiber diameter of 149±47 nm, which was similar to the CS/PEO nanofibers with the diameter of 140.9±24.8 nm previously spun by Deng *et al.* [26]. It could be found that the fibers containing TTOLs had a few burrs and the fiber diameter increased when TTOLs were added into the spinning solution (Figure 2(D)). This might be due to the hydrophobicity and non-polarity of TTOLs, the electrostatic interaction of negative charges on the surface of TTOLs and the positive charges of chitosan (Figure S1), which reduced the charge density of spinning solutions and decreased the tensile force exerted by jet injection under the action of electric field, resulting in thick fibers.

From IR and XRD spectra, the types of the interaction between molecules and functional groups in the three materials have no significant difference in Figure S2(A) and (B). From the DSC data in Figure S2(C), the endothermic peak decreases and moves forward in the TTO-CENs and TOL-CENs due to the weaker binding force between TTO and the material, followed by a small endothermic peak.

Physicochemical Performance of Polymer Materials

Porosity is a fundamental structural parameter of ANMs,

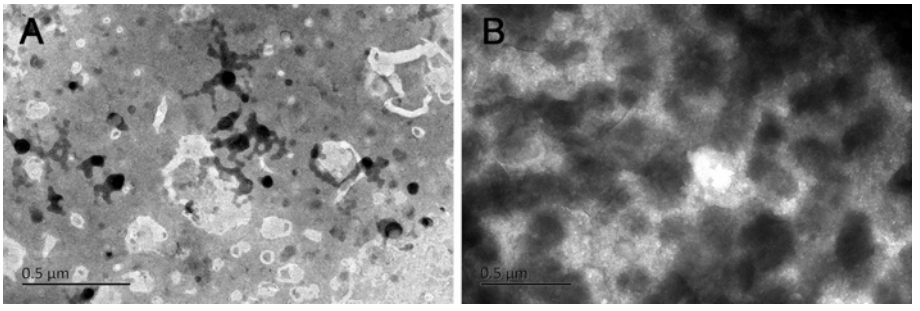

Figure 1. The morphology of TTOLs before (A) and after (B) mixing with the polymer solution (4.0 wt% polymer concentration, the mass ratio of chitosan to PEO=90:10). 2.0 vt% TTOLs was added into the polymer solution.

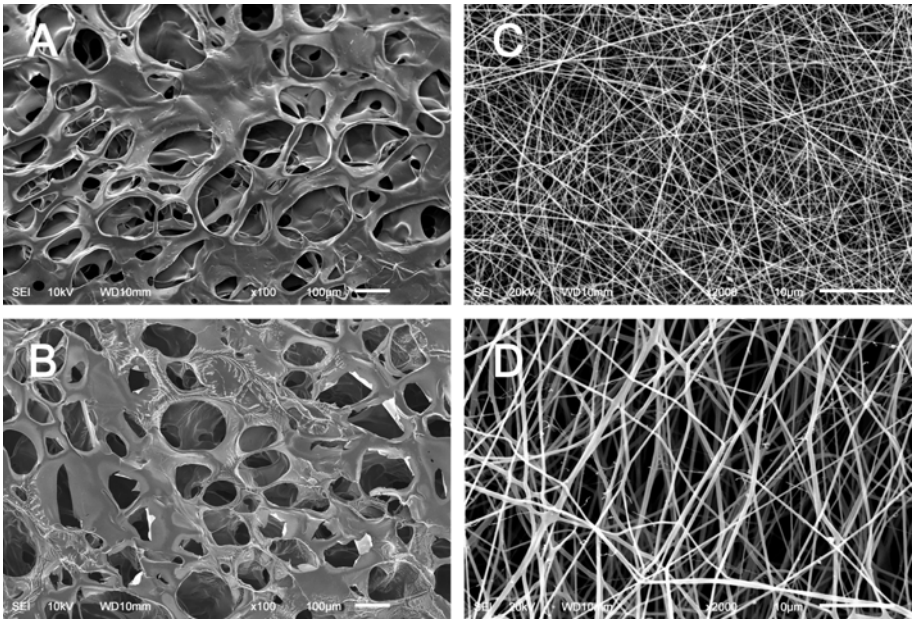

Figure 2. SEM micrographs of (A) CFSs, (B) TOL-CFSs, (C) CENs, and (D) TOL-CENs.

which determines physicochemical properties, such as fluid absorption and air permeability [40]. According to the data presented in Table 1, the porosity of TTO-CENs and TOL-CENs is much larger, and increases by about 45 % compared with TTO-CFSs and TOL-CFSs. Moreover, the addition of TTOLs in CENs slightly decreased the porosity in the comparation of TTO addition. It might be the fact that the negative charges on the surface of TTOLs were neutralized with the positive charges of chitosan in spinning process, which led to the increase in fiber diameter. FA and WVTR of chitosan-based ANMs mainly depended on the porosity, so FA and WVTR of TTO-CENs and TOL-CENs gradually increased with the increase of porosity. Perhaps for the same reason, the incorporation of TTOLs caused a slighter decrease in FA and WVTR of materials than TTO, but there was no significant statistical difference. Compared with CFSs, the tensile strength and Young's modulus of CENs are significantly reduced by 79.76±9.42 % and 62.44±8.56 % for TTO addition, 81.31±13.92 % and 46.44±5.73 % for TTOLs, respectively. It was caused by the lower areal density in cross section of CENs due to high porosity and small fiber diameter of materials. Their elongation at break also increases by about 4.24 and 5.87 times, respectively. This showed that CENs were more flexible and elastic, which was helpful to the application of materials in mechanical stress environment.

In vitro Terpinen-4-ol Release of TOL-CENs

Figure 3 shows the release of terpinen-4-ol from TTO-CFSs, TTO-CENs, TOL-CFSs and TOL-CENs. Terpinen-4-ol in the TTO-CFSs and TTO-CENs quickly diffused to the outside of materials, and the outward diffusion of terpinen-4-ol was equal to the inward diffusion, establishing the balance of release system after 2 h of the release. The main reason was that terpinen-4-ol mainly existed in the free form in the interior of material due to the lack of liposome encapsulation. It had higher concentration of free terpinen-4-ol and porosity compared to the other composite materials. As the chitosan-based materials swelled, the diffusion rate of drug became faster. Despite of the large porosity of TOL-CFSs, the encapsulation of TTO caused by liposomal membrane retarded the terpinen-4-ol release. TTO was also encapsulated by

Table 1. The porosity, fluid absorptivity, water vapor transmission rate, tensile strength, Young's modulus and elongation at break of TTO-CFSs, TOL-CFSs, TTO-CENs and TOL-CENs

Sample	Porosity (%)	FA ($g \cdot g^{-1}$)	WVTR ($g \cdot m^{-2} \cdot d^{-1}$)	Tensile strength (MPa)	Young's modulus (MPa)	Elongation at break (%)
TTO-CFSs	68.3±1.0	8.52±0.46	1023±61	2.52±0.24	6.31±0.33	5.4±1.8
TOL-CFSs	65.2±0.8	7.97±0.32	1009±58	2.14±0.29	5.34±0.25	4.7±1.5
TTO-CENs	98.6±1.1	18.94±0.72	2613±48	0.51±0.31	2.37±0.43	28.3±5.9
TOL-CENs	97.4±0.7	18.91±0.19	2589±60	0.40±0.17	2.86±0.52	32.3±6.8

liposomes in TOL-CENs to prevent the rapid release of terpinen-4-ol. However, owing to the larger porosity and specific surface area of TOL-CENs, the terpinen-4-ol release was faster than TOL-CFSs. Therefore, it was possible to maintain the higher concentration of terpinen-4-ol in the external environment than TOL-CFSs, which was essential for the maintenance of efficient antimicrobial effects in long-term service.

Study of Drug-release Kinetics and Mechanism of Drug Release

In order to completely explain the kinetics of drug release, the terpinen-4-ol release curve in TOL-CFSs and TOL-CENs (Figure 3) was fitted by the five release kinetic models including zero order, first order, Hixson-Crowell, Higuchi and modified Korsmeyer-Peppas model. The value of regression coefficient (R^2) from *in vitro* drug release are determined so that it can evaluate which a particular model is being followed. The regression values obtained for both type of polymer carrier are reported in Table 2. In the five models studied, the modified Korsmeyer-Peppas release model was found more followed in case of both TOL-CFSs and TOL-CENs. This indicated that terpinen-4-ol release was mainly controlled by diffusion-controlled release mechanism and swelling mechanism of polymer matrix [42-44].

The mechanism of terpinen-4-ol release was studied using modified Korsmeyer-Peppas model. This model explains that whether release pattern follows Fickian diffusion or not. The values of release rate constant (k) and release exponent (n) obtained for each of the formulations are mentioned in Table 3. The release index n of two types is less than 0.45 and release mechanism is dominated by Fickian diffusion. Compared with the burst effects (M_0) of the four materials in Figure 3, TTO was directly incorporated into the polymer carrier in TTO-CFSs and TTO-CENs and free terpinen-4-ol triggered the significant burst effect. The results displayed more than 90 % release of the initial terpinen-4-ol in TTO-CFSs and TTO-CENs for 2 h. On the contrary, the components of TTO were encapsulated by liposomal phospholipid bilayer in TOL-CFSs and TOL-CENs, so the burst effects are only 1.84 % and 3.88 %, respectively. TTO components were lipophilic so that the proportionate distribution of them between the liposomal phospholipid bilayer and polymer layer outside of liposomes occurred according to the distribution law (Figure S3) [29]. The octanol-water partition coefficient of terpinen-4-ol was 3.26 [15], which was inferred that c_{max} was about 1800 times that of c_R. Hence, liposomal encapsulation reduced the concentration gradient of terpinen-4-ol outwards, greatly decreasing the mass transfer rate of terpinen-4-ol to the outside of liposomes and the burst effects of material.

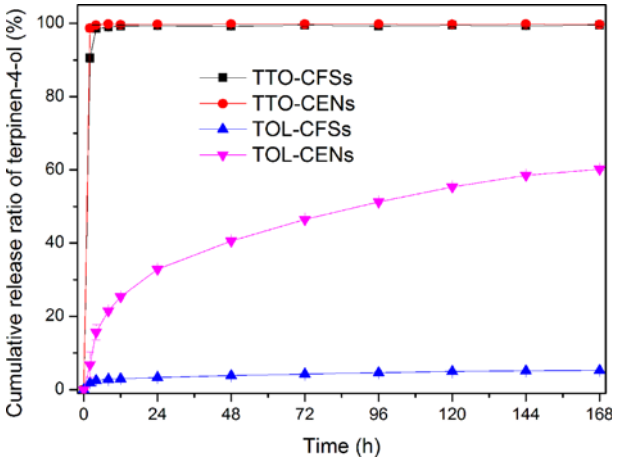

Figure 3. Terpinen-4-ol release profile of TTO-CFSs, TTO-CENs, TOL-CFSs and TOL-CENs.

Table 3. The release rate constant (k), the release exponent (n) and the initial terpinen-4-ol released ratio (M_0) obtained for drug formulation of modified Korsmeyer-Peppas model fitting

Sample	k	n	M_0
TOL-CFSs	0.4566	0.3962	1.836
TOL-CENs	12.3304	0.3126	3.882

Effect of Different Parameters on Terpinen-4-ol Release Behavior of TOL-CENs

In order to investigate the influencing factors on terpinen-4-ol release behavior of TOL-CENs, the TOL-CENs containing different TTOLs concentrations (1.0 vt%, 1.5 vt%, 2.0 vt%, 2.5 vt%, 3.0 vt%), polymer concentrations (3.0 wt%, 3.5 wt%, 4.0 wt%, 4.5 wt%, 5.0 wt%), the mass ratio of chitosan to PEO (90:10, 80:20, 70:30, 60:40, 50:50) and crosslinker (genipin) concentrations (0.20 mg/m*l*, 0.25 mg/m*l*, 0.30 mg/m*l*, 0.35 mg/m*l*, 0.40 mg/m*l*) were prepared to determine the cumulative terpinen-4-ol release from TOL-CENs.

TTOLs play an important role in antimicrobial ability of materials. TTOLs concentration has vital effects on the long-term antimicrobial property. Figure 4(A) shows the effect of TTOLs loading on terpinen-4-ol release from TOL-CENs. With the improvement of TTOLs concentration, the cumulative

Table 2. Kinetic profile of terpinen-4-ol release from TOL-CFSs and TOL-CENs

Sample	Zero order	First order	Hixson-Crowell	Higuchi	modified Korsmeyer-Peppas
TOL-CFSs	0.7349	0.6791	0.8594	0.9954	0.9990
TOL-CENs	0.8418	0.2770	0.9415	0.9898	0.9997

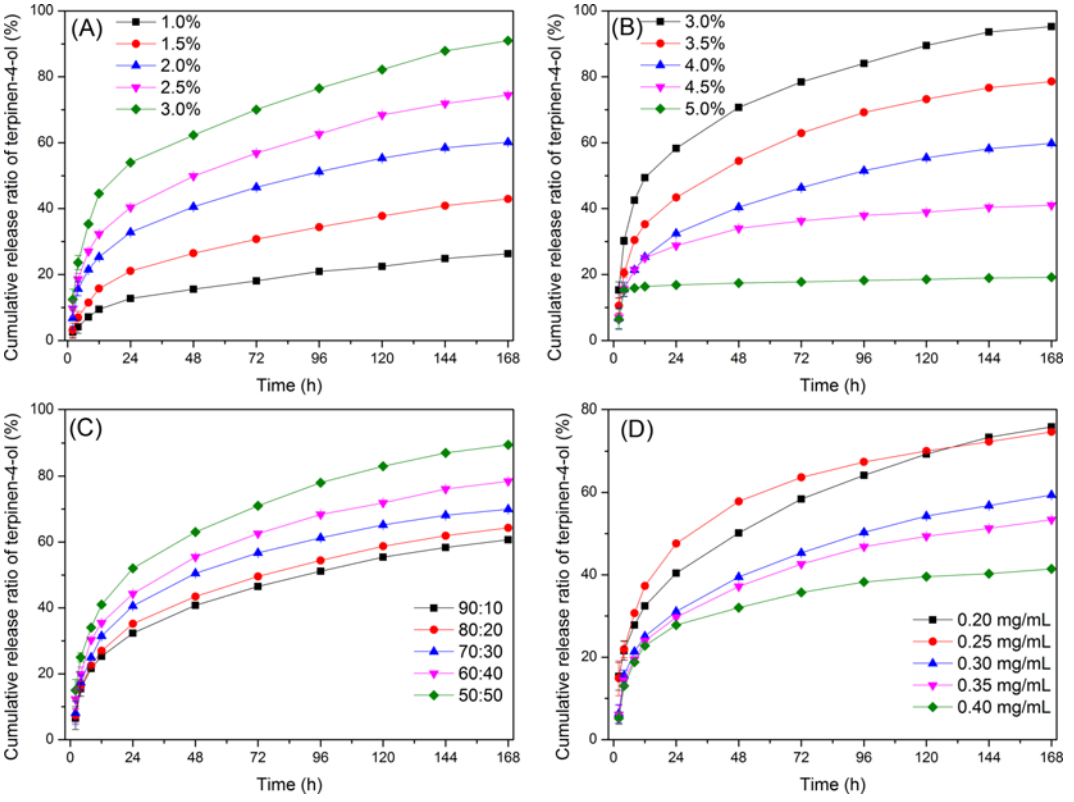

Figure 4. Effect of TTOLs concentrations, polymer concentrations, the mass ratio of chitosan to PEO and crosslinker concentrations on terpinen-4-ol release of the TOL-CENs; (A) TTOLs concentrations (4.0 wt% polymer concentration, the mass ratio of chitosan to PEO=90:10), (B) polymer concentrations (2.0 vt% TTOLs concentration, the mass ratio of chitosan to PEO=90:10), (C) the mass ratio of chitosan to PEO (2.0 vt% TTOLs concentration, 4.0 wt% polymer concentration), and (D) crosslinker (genipin) concentrations (2.0 vt% TTOLs concentration, 4.0 wt% polymer concentration, the mass ratio of chitosan to PEO=90:10).

terpinen-4-ol release rate gradually increased at the same time. The reason was probably that the increase of TTOLs loading reversed the ratio of chitosan to liposome and TTOLs gradually become saturated so that TTOLs might be excessive, causing the increased free TTOLs to enhance the burst effect. Moreover, the stability of liposomes depended on the electrostatic attraction of chitosan around itself to form a self-assembled structure. Excessive TTOLs interfered with the self-assembly structure and further accelerated the terpinen-4-ol release.

Polymer is the skeleton of materials and chitosan can stabilize TTOLs in the polymer. The results of terpinen-4-ol release from the TOL-CENs with different polymer concentration are shown in Figure 4(B). With the improvement of polymer concentration, the burst effect of the material gradually decreased. The initial cumulative release rate of terpinen-4-ol from the TOL-CEN with 3.0 wt% to 5.0 wt% polymer dropped from 15.34 % to 6.44 % for 2 h. After the burst effect, the higher the polymer concentration was, the more stable TTOLs was, resulting in the slow terpinen-4-ol release rate owing to electrostatic interaction in self assembly.

Similar to the effect of polymer concentrations on terpinen-4-ol release, the ratio of chitosan to PEO in the polymer is relative to chitosan concentration, which affects the stability of TTOLs and thus the release behavior. As shown in Figure 4(C), the burst effect of terpinen-4-ol release significantly enhanced with the decreased mass ratio of chitosan to PEO. The probable reason was that the decreased chitosan proportion weakened the electrostatic interaction of chitosan and TTOLs and slightly increased the terpinen-4-ol release rate. At a constant CS/PEO ratio, chitosan concentration varies with the polymer concentration in the same proportion. But when polymer concentration is constant, the reduction degree in chitosan concentration caused by the decrease of CS/PEO ratio is much smaller. Therefore, the changes in release rate of terpinen-4-ol caused by the mass ratio of chitosan to PEO was weaker than polymer concentration.

Genipin is an aglycone derived from an iridoid glycoside called geniposide present in fruit of *Gardenia jasminoides*. Genipin has strong cross-linking ability, good biocompatibility and is hardly degradable and non-toxic [48]. Genipin can spontaneously crosslink with the free amino groups of chitosan to produce a kind of dark blue pigments in the form

of single or multiple molecules. The linear chitosan molecules are cross-linked together to form the network structure so that the strength and elasticity of nanofiber mats are improved [49,50]. A certain amount of genipin was added into the spinning solution before electrospinning and the crosslinked TOL-CENs was obtained after left overnight at 40 °C. Figure 4(D) represents the effect of crosslinker concentrations on terpinen-4-ol release from TOL-CENs. The addition of a small amount of cross-linking agents (<0.25 mg/m*l*) accelerated terpinen-4-ol release. The reason was probably that the combination of cross-linking agents with the amino groups of chitosan disrupted the electrostatic interaction between chitosan and the liposomal phospholipid

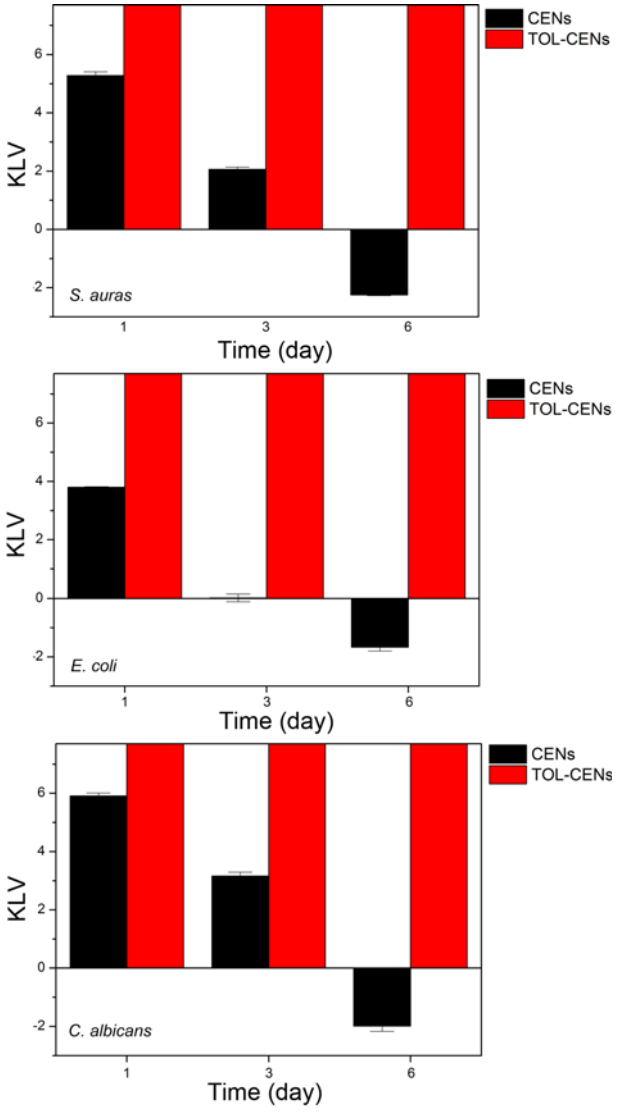

Figure 5. KLV of CENs and TOL-CENs against *S. aureus*, *E. coli* and *C. albicans* (CENs: 4.0 wt% polymer concentration, the mass ratio of chitosan to PEO=90:10; TOL-CENs: 2.0 vt% TTOLs, 4.0 wt% polymer concentration, the mass ratio of chitosan to PEO=90:10).

outer layer, and interfered the self-assembly structure, causing the liposome instability and rapid release of terpinen-4-ol. However, when the amount of cross-linking agents was more than 0.30 mg/m*l*, the crosslink of cross-linking agents and chitosan solidified liposomes, which might re-stabilize the liposomes, preventing the release of terpinen-4-ol. As the amount of cross-linking agents increased, the release rate of terpinen-4-ol gradually slowed down.

Long-term Bactericidal Capability of TOL-CENs

KLV is used to assess long-term bactericidal effects of TOL-CENs and it is determined on the basis of the described method. KLVs of CENs against *S. aureus*, *E. coli* and *C. albicans* are 5.28, 3.80 and 5.91 after treatment for one day in Figure 5, indicating that chitosan-based nanofiber mats has a role in killing three microorganisms. However, as the treatment time increased, the microbiocide effect gradually decreased. The proliferation rate of cells was fast and gradually exceeded the death rate in the eutrophic culture medium. In addition, the adsorption of amino cations of chitosan reached the saturation so that to eliminate the microbiocide effect of materials. By 6 days, the number of live cells exceeded the initial number of cells. KLVs seen in Figure 5 are all less than zero. Compared with CENs, the antimicrobial efficiency of TOL-CENs is improved after incorporating TTOLs, whose KLVs against *S. aureus*, *E. coli* and *C. albicans* exceed 7.70 (killing all cells of microorganisms) after treating for one day, exhibiting excellent killing efficiency. Moreover, the microbiocide effects continued until day 6. The combination of liposome-encapsulated TTO and CS/PEO nanofibers can reveal significant bactericidal effect, which indicates that essential oil liposomes play an important role in antimicrobial capability.

TEM of Microbial Cells

In order to further demonstrate the bactericidal mechanism of TOL-CENs, TEM was used to analyze the changes in submicroscopic structure of microorganisms before and after the treatment of TOL-CENs. According to Figure 6, *S. aureus*, *E. coli* and *C. albicans* in the control group display the normal form and structure, namely grapevine, short-rod-shaped and oval structure, respectively. After being treated with CENs, the cell plates of *S. aureus* disappeared, but cell structure was still intact without size changes, indicating that chitosan-based nanofibers could inhibit the formation of cell plate in the mitosis and hamper the proliferation of *S. aureus*. Additionally, a transparent zone appeared around *E. coli* treated with CENs, and the aggregates with different sizes also occurred in cells. It might be in virtue of the fact that the cell walls of *E. coli* contained teichoic acid, lipids and polysaccharides, which all had negative charges after ionization. The amino cations of chitosan combined with these substances, destroyed cell walls and cell membranes, caused the changes in osmotic pressure of cells and formed a

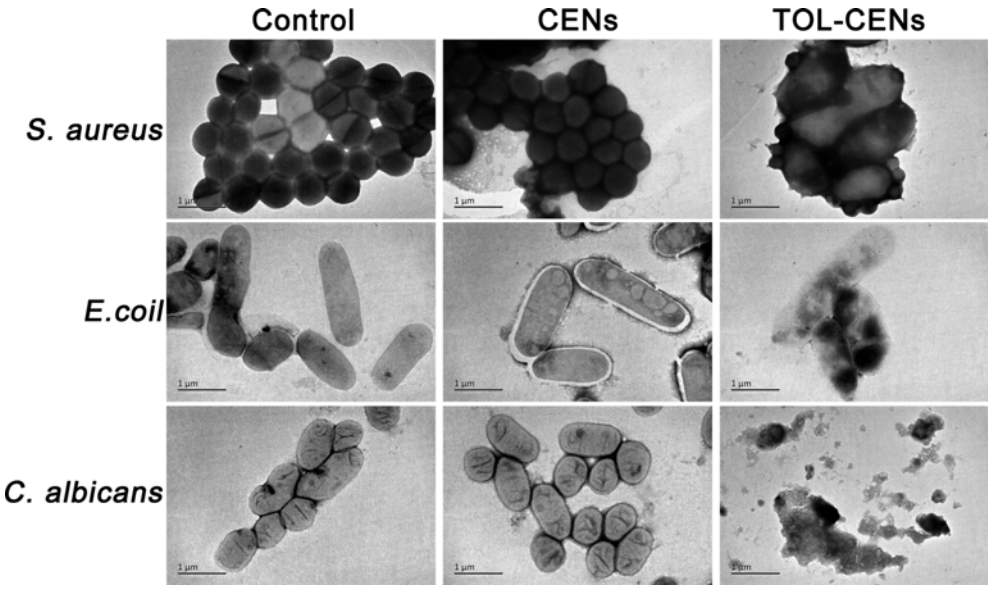

Figure 6. TEM photography of *S. aureus*, *E. coli* and *C. albicans* treated with CENs and TOL-CENs for 24 h, respectively (CENs: 4.0 wt% polymer concentration, the mass ratio of chitosan to PEO=90:10; TOL-CENs: 2.0 vt% TTOLs, 4.0 wt% polymer concentration, the mass ratio of chitosan to PEO=90:10).

transparent zone and the aggregates. This was consistent with the results reported by Helander, who observed *E. coli* treated with chitosan by SEM and also found that chitosan encapsulated the outer cell membrane in the small vesicle structure, resulting in the changes in whole cell surface [51]. In the case of *C. albicans*, There were no obvious changes in the structure of individual cells after being treated with CENs. But the adhesion and connection among cells changed, the pseudohyphatic structure was destroyed. The cells were arranged irregularly and formed the clusters. Previous research has suggested that chitosan could hinder the biomembrane formation of *C. albicans* during the process of cell adhesion by inhibiting the metabolic activity of *C. albicans* [52]. After treated with TOL-CENs, the ultrastructures of three microbes were siginificantly changed. The cell membranes and walls of *S. aureus* and *C. albicans* were completely disintegrated and the contents of cells outflowed. The cell boundary of *E. coli* disappeared and the maldistribution of cytoplasm occurred. The results were consistent with the previous results of TTOLs/CS composite sponges [40]. TOL-CENs should have similar microbicidal mechanism, including the synergistic microbicidal mechanism of chitosan and TTOLs and the re-encapsulation cycle mechanism of TTO [40].

Conclusion

In conclusion, TOL-CENs were fabricated using TTOLs as an antimicrobial agent and electrospinning. It was observed by SEM that the fiber diameter was enlarged caused by incorporation of TTOLs into chitosan-based nanofibers. Owing to the large porosity, TOL-CENs had good fluid absorption and water vapor permeability, and also exhibited excellent mechanical strength and flexibility. The interaction of TTOLs and chitosan played a decisive role on the controlled release of terpinen-4-ol. TOL-CENs could maintain high terpinen-4-ol level in the external environment and demonstrate remarkable long-term microbicidal capability against *S. aureus*, *E. coli* and *C. albicans*. Based on the above advantages of performances, the developed TOL-CENs would represent a valuable alternative for ANMs.

Acknowledgements

This work was supported by National Natural Science Foundation of China (grant no. 51803095), Natural Science Research of Jiangsu Higher Education Institutions of China (grant no. 17KJB540002).

Electronic Supplementary Material (ESM) The online version of this article (doi: 10.1007/s12221-019-1092-1) contains supplementary material, which is available to authorized users.

References

1. Y. Ren, J. Guo, Q. Lu, D. Xu, J. Qin, and F. Yan, *Chemsuschem*, **11**, 1092 (2018).
2. Y. Zhu, C. Xu, N. Zhang, X. Ding, B. Yu, and F.-J. Xu, *Adv. Funct. Mater.*, **28**, 1706709 (2018).
3. T. V. Ivanova, R. Krumpolec, T. Homola, E. Musin, G. Baier, K. Landfester, D. C. Cameron, and M. Cernak,

Plasma Processes Polym., **14**, e1600231 (2017).
4. I. Yousefi, M. Pakravan, H. Rahimi, A. Bahador, Z. Farshadzadeh, and I. Haririan, *Mat. Sci. Eng. C-Mater.*, **75**, 433 (2017).
5. C. Kriegel, A. Arrechi, K. Kit, D. J. McClements, and J. Weiss, *Crit. Rev. Food Sci. Nutr.*, **48**, 775 (2008).
6. H. Cui, J. Wu, C. Li, and L. Lin, *LWT - Food Sci. Technol.*, **81**, 233 (2017).
7. L. Lin, Y. Zhu, C. Li, L. Liu, D. Surendhiran, and H. Cui, *Carbohydr. Polym.*, **198**, 225 (2018).
8. H. Cui, M. Bai, and L. Lin, *Carbohydr. Polym.*, **179**, 360 (2018).
9. M. Sadri, S. Arab-Sorkhi, H. Vatani, and A. Bagheri-Pebdeni, *Fiber. Polym.*, **16**, 1742 (2015).
10. S. Degoutin, M. Jimenez, F. Chai, T. Pinalie, S. Bellayer, M. Vandenbossche, C. Neut, N. Blanchemain, and B. Martel, *J. Biomed. Mater. Res. A*, **102**, 3846 (2014).
11. N. Naveen, R. Kumar, S. Balaji, T. S. Uma, T. S. Natrajan, and P. K. Sehgal, *Adv. Eng. Mater.*, **12**, B380 (2010).
12. N. E. Zander, M. Gillan, and D. Sweetser, *Materials*, **9**, 247 (2016).
13. X. Deng, A. Nikiforov, D. Vujosevic, V. Vuksanovic, B. Mugosa, U. Cvelbar, N. De Geyter, R. Morent, and C. Leys, *Mater. Lett.*, **149**, 95 (2015).
14. H. Rokbani, F. Daigle, and A. Ajji, *Nanomaterials*, **8**, 129 (2018).
15. C. F. Carson, K. A. Hammer, and T. V. Riley, *Clin. Microbiol. Rev.*, **19**, 50 (2006).
16. M. Sherry, C. Charcosset, H. Fessi, and H. Greige-Gerges, *J. Liposome Res.*, **23**, 268 (2013).
17. B. M. Hausen, *Dermatitis*, **15**, 213 (2004).
18. B. M. Hausen, J. Reichling, and M. Harkenthal, *Am. J. Contact Dermat.*, **10**, 68 (1999).
19. Y. Ge and M. Q. Ge, *J. Liposome Res.*, **25**, 222 (2015).
20. A. M. Abdelgawad, S. M. Hudson, and O. J. Rojas, *Carbohydr. Polym.*, **100**, 166 (2014).
21. J. S. Choi, K. W. Leong, and H. S. Yoo, *Biomaterials*, **29**, 587 (2008).
22. K. Ohkawa, D. I. Cha, H. Kim, A. Nishida, and H. Yamamoto, *Macromol. Rapid Commun.*, **25**, 1600 (2004).
23. X. Y. Geng, O. H. Kwon, and J. H. Jang, *Biomaterials*, **26**, 5427 (2005).
24. B. M. Min, S. W. Lee, J. N. Lim, Y. You, T. S. Lee, P. H. Kang, and W. H. Park, *Polymer*, **45**, 7137 (2004).
25. B. Duan, C. H. Dong, X. Y. Yuan, and K. D. Yao, *J. Biomaterials Sci-polym. E.*, **15**, 797 (2004).
26. L. Deng, M. Taxipalati, A. Zhang, F. Que, H. Wei, F. Feng, and H. Zhang, *J. Agr. Food Chem.*, **66**, 6219 (2018).
27. D. Wang, Q. Lu, M. Wei, and E. Guo, *J. Appl. Polym. Sci.*, **135**, 46504 (2018).
28. R. X. Wu, G. F. Zheng, W. W. Li, L. B. Zhong, and Y. M. Zheng, *J. Nanosci. Nanotechnol.*, **18**, 5624 (2018).
29. Y. Ge and M. Q. Ge, *J. Exp. Nanosci.*, **11**, 345 (2015).
30. R. Bnyan, I. Khan, T. Ehtezazi, I. Saleem, S. Gordon, F. O'Neill, and M. Roberts, *J. Pharm. Sci.*, **107**, 1237 (2018).
31. K. B. Johnsen, J. M. Gudbergsson, M. Duroux, T. Moos, T. L. Andresen, and J. B. Simonsen, *J. Control. Release*, **269**, 10 (2018).
32. C. Liolios, O. Gortzi, S. Lalas, J. Tsaknis, and I. Chinou, *Food Chem.*, **112**, 77 (2009).
33. C. Sinico, A. De Logu, F. Lai, D. Valenti, M. Manconi, G. Loy, L. Bonsignore, and A. M. Fadda, *Eur. J. Pharm. Biopharm.*, **59**, 161 (2005).
34. E. Moghimipour, N. Aghel, A. Zarei Mahmoudabadi, Z. Ramezani, and S. Handali, *Jundishapur J. Nat. Pharm. Prod.*, **7**, 117 (2012).
35. H. Cui, L. Yuan, W. Li, and L. Lin, *Int. J. Food Sci. Tech.*, **52**, 687 (2017).
36. H. Cui, M. Bai, M. M. A. Rashed, and L. Lin, *Int. J. Food Microbiol.*, **266**, 69 (2018).
37. L. Lin, Y. Dai, and H. Cui, *Carbohydr. Polym.*, **178**, 131 (2017).
38. L. Lin, Y. Zhu, and H. Cui, *Lwt-Food Sci. Technol.*, **97**, 711 (2018).
39. H. Cui, M. Bai, C. Li, R. Liu, and L. Lin, *LWT - Food Sci. Technol.*, **96**, 671 (2018).
40. Y. Ge and J. P. Tang, *Fiber. Polym.*, **17**, 862 (2016).
41. J. P. Tang and Y. Ge, *Fiber. Polym.*, **18**, 424 (2017).
42. J. L. Ford, K. Mitchell, P. Rowe, D. J. Armstrong, P. N. Elliott, C. Rostron, and J. E. Hogan, *Int. J. Pharm.*, **71**, 95 (1991).
43. H. Kim and R. Fassihi, *J. Pharm. Sci.*, **86**, 316 (1997).
44. H. Kim and R. Fassihi, *J. Pharm. Sci.*, **86**, 323 (1997).
45. C. Y. Gao, D. Y. Wang, and J. C. Shen, *Polym. Adv. Technol.*, **14**, 373 (2003).
46. G. Chen, T. Ushida, and T. Tateishi, *Mat. Sci. Eng. C-Mater.*, **17**, 63 (2001).
47. G. Dogan, F. Ozyildiz, G. Basal, and A. Uzel, *Int. Polym. Process*, **28**, 143 (2013).
48. A. J. Bavariya, A. Norowski, Jr., K. M. Anderson, P. C. Adatrow, F. Garcia-Godoy, S. H. Stein, and J. D. Bumgardner, *J. Biomed. Mater. Res. B*, **102**, 1084 (2014).
49. M. E. Frohbergh, A. Katsman, G. R. Botta, P. Lazarovici, C. L. Schauer, U. G. K. Wegst, and P. I. Lelkes, *Biomaterials*, **33**, 9167 (2012).
50. K. Jalaja, D. Naskar, S. C. Kundu, and N. R. James, *Carbohydr. Polym.*, **136**, 1098 (2016).
51. I. M. Helander, E. L. Nurmiaho-Lassila, R. Ahvenainen, J. Rhoades, and S. Roller, *Int. J. Food Microbiol.*, **71**, 235 (2001).
52. L. G. Silva Garcia, G. M. de Melo Guedes, M. L. Queiroz da Silva, D. S. Collares Maia Castelo-Branco, J. J. Costa Sidrim, R. d. A. Cordeiro, M. F. Gadelha Rocha, R. S. Vieira, and R. S. Nogueira Brilhante, *Carbohydr. Polym.*, **195**, 662 (2018).